

Efficient Transition State Searches by Freezing String Method with Graph Neural Network Potentials

Jonah Marks¹ and Joseph Gomes¹*Department of Chemical and Biochemical Engineering, University of Iowa, Iowa City, United States*

(*Electronic mail: joe-gomes@uiowa.edu)

(Dated: 13 January 2025)

Transition states are a critical bottleneck in chemical transformations. Significant efforts have been made to develop algorithms that efficiently locate transition states on potential energy surfaces. However, the computational cost of *ab-initio* potential energy surface evaluation limits the size of chemical systems that can routinely studied. In this work, we develop and fine-tune a graph neural network potential energy function suitable for describing organic chemical reactions and use it to rapidly identify transition state guess structures. We successfully refine guess structures and locate a transition state in each test system considered and reduce the average number of *ab-initio* calculations by 47% through use of the graph neural network potential energy function. Our results show that modern machine learning models have reached levels of reliability whereby they can be used to accelerate routine computational chemistry tasks.

I. INTRODUCTION

Knowledge of transition states (TS) is vital to accurately characterizing chemical reactions and predicting thermodynamic and kinetic rate parameters. However, TS are difficult to locate; they exist as first-order saddle points on the Born-Oppenheimer potential energy surface (PES) of atomic systems. To address the challenge of locating TS, a variety of algorithms and methods have been developed. TS search algorithms use first derivative (often referred to as density functional theory (DFT) calculations) and Hessian information to explore the PES and locate the TS, but this requires a suitable guess structure and a significant number of PES evaluations in series.

TS search methods can be broadly categorized into surface walking¹⁻⁵ methods and interpolation-based methods. Surface-walking algorithms maximize the largest negative eigenvalue of the Hessian matrix by moving uphill to locate the saddle point associated with that vibrational mode. In contrast, interpolation-based methods often split the search into two steps, leveraging two different algorithms. The first step of the interpolation-based approach is to use a non-local path finding algorithm to obtain a TS guess structure by efficiently stepping across the PES using only first derivative information. In the second step, the TS guess structure is used as the starting point for a surface walking algorithm to locate the exact TS.

The success and efficiency of the overall search are heavily dependent on non-local path-finding algorithm; guess structures close to the saddle point of interest will quickly converge, minimizing the number of Hessian calculations required. However, guess structures that lie outside the basin of attraction will cause the surface walking algorithm to converge to an off-target critical point or fail to converge entirely.

Development of reliable and efficient interpolation methods is a longstanding area of research. Early chain of states methods step across the PES to create a series of intermediate geometries connecting reactant and product⁶⁻⁸. The string method⁹ and the Nudged Elastic Band (NEB)¹⁰⁻¹⁶ are dou-

ble ended chain-of-states methods for estimating TS. These methods give information about the approximate minimum energy pathway and barrier height. Growing string methods construct an improved initial pathway from which a TS guess can be obtained by iteratively adding and optimizing intermediate structures^{17,18}. This allows the algorithm to avoid DFT calculations in non-physical areas of chemical space that initial interpolation paths may traverse.

Reducing the computational cost of TS searches through algorithmic improvements to the reliability¹⁹⁻²³ and interpolation methods²⁴⁻²⁶ of TS searches continues to be an area of active research. These improvements have reduced the number of PES evaluations required to approximate the TS from thousands to under 100 DFT calculations²⁷.

Despite recent advancements in TS search algorithms, the underlying cost of the PES cannot be averted. Historically, potential energy functions trade level of detail for computational cost²⁸⁻³². Inexpensive methods like atomic force fields, while efficient^{33,34}, do not include sufficient detail to accurately describe chemical reactions. In some notable exceptions³⁵⁻³⁷ reactive behavior can be parameterized into force fields; however, these methods are often fit to specific system types and are not broadly applicable when compared to quantum chemistry techniques like DFT. DFT predicts the potential energy of a system as a function of electron density by approximating the solution to the Schrödinger equation. This gives accurate molecular property information enabling simulation of reactive behavior. DFT scales non-linearly with respect to system size, placing a practical limit on system size that can be considered. Within DFT, exchange correlation (xc) functionals and basis set pairs determine the cost and accuracy of a simulation with more accurate xc functional/basis pairs incurring higher computational cost. One strategy to reduce TS search cost leverages this continuum by performing a TS search with a lower level of theory before re-calculating the final results at a higher level of theory^{38,39}. Another method estimates the topology of the PES via interpolation to reduce the number of DFT calculations⁴⁰.

In recent decades machine learning (ML) models have proven to be powerful emulators of physics-based calcula-

tions (like DFT). Once trained, ML models require a fraction of the computational resources and exhibit favorable scaling with respect to system size. Early ML-based potentials, while innovative, failed to achieve chemical accuracy (error < 2kcal/mol) across relevant areas of chemical space and were often fit to individual molecular systems, limiting broader applicability^{28,41,42}. In contrast, modern ML models excel at approximating functions from large quantities of data. Several classes of neural network potentials (NNP) have emerged as computationally efficient approximators to expensive simulations like DFT: Behler-Parinello networks^{28,43,44}, message passing neural networks⁴⁵⁻⁴⁸, and equivariant networks⁴⁹⁻⁵¹.

However, NNPs are heavily dependent on training data. Current datasets^{52,53} accurately describe minimum energy geometries and minorly perturbed structures. Training on these datasets results in models that achieve chemical accuracy on minimum or near-minimum structures^{43,44,47}. This has enabled incorporation of ML potential energy functions into routine computational chemistry tasks like molecular dynamics^{28,54,55} and geometry optimizations^{56,57}. However, accurate prediction of reaction parameters requires description of the TS, which lies in an area of chemical space inadequately described by current datasets. Consequently, models trained on current datasets are unable to accurately predict the potential energy and forces along reaction pathways prohibiting their use in classical reaction simulations^{58,59}. Application of active learning and enhanced sampling methods has resulted in configurationally diverse datasets⁵⁹⁻⁶³. Small datasets of reaction pathways⁵⁸ and critical points of reactions⁶⁴ have been published in recent years, but these datasets are of insufficient size to fully train modern ML potentials. Thus, despite the rapid advancement and incorporation of ML into computational chemistry, application of ML to TS searches has had limited success.

In recent years, directly predicting reaction parameters, such as enthalpy of reaction, barrier heights, or TS geometry, from reactant and product structures/descriptors has been an area of significant research⁶⁵⁻⁷⁵. However, these methodologies are often limited in scope and are unable to reach chemical accuracy across broad benchmark test sets.

Incorporation of ML potential energy functions into classical TS searches is a more universal approach. In classical TS searches the process is broken into discrete steps that use well understood techniques like geometry optimization, PES exploration algorithms, and saddle point search algorithms^{4,5,76-81}. Substituting a ML PES for a classical *ab-initio* PES in one or more of these tasks significantly reduces the computational cost of the TS search. This has been achieved through construction of approximate PES via Gaussian Process (GP) regression⁸²⁻⁸⁵. While this methodology accelerates the overall TS search, the GP is fit on the fly to a given chemical system which requires *ab-initio* calculations and cannot generalize to other systems; each TS search requires fitting a new GP from scratch.

Two notable methods that incorporate ML PES into classical TS searches are CaTsunami and NeuralNEB. Both perform TS searches using pre-trained ML potentials and require no *ab-initio* calculations to obtain a TS guess geometry. Both

methods also use the NEB method with ML potential energy functions^{86,87}, significantly reducing the computational cost of the NEB calculation. However, the additional error introduced by the ML potential energy function lowers the success rate of the TS searches. The authors of CaTsunami examine failed TS searches and find high root-mean-squared-error (RMSE) in relative potential energy predictions along the NEB path. Models trained on equilibrium data⁵² perform far worse than models trained on configurationally diverse datasets⁵⁸, as reaction mechanisms often pass areas of chemical space that are rarely sampled.

In this work, we successfully demonstrate the incorporation of a graph neural network (GNN) PES into a different automated TS search algorithm: the freezing string method (FSM)¹⁸. First, we train SchNet⁴⁷ on the ANI-1 dataset⁵³. This model accurately describes normal mode perturbed molecular structures, although we find that it is not sufficient for TS searches as it poorly describes regions of chemical space where TS exist. In the second training step, we improve our model by fine-tuning on a small dataset of reactants, TS, and products. We use the final fine-tuned model to perform FSM calculations for a benchmark set of well studied organic elementary reactions. We find that incorporation of GNN potential energy functions into the FSM significantly reduces the computational cost of TS searches while maintaining a high TS search success rate. This work suggests that with appropriate pre-training, modern ML potential energy functions have reached a level of accuracy sufficient to be incorporated into routine computational chemistry tasks where computational cost is limiting factor.

II. METHODS

A. Datasets

In this work, we use the ANI-1 Dataset⁵³ to pre-train a GNN potential energy function. The ANI-1 dataset contains approximately 20M off-equilibrium conformers of 57k molecules drawn from the GDB-11^{88,89} database of organic molecules. The molecules selected contain up to 8 heavy (C-N-O) atoms with corresponding hydrogen atoms required to make molecules with neutral charge and a singlet electronic ground state. All structures and energies of the ANI-1 dataset are calculated at the ω B97X/6-31G(d) level of theory. The structures included in the ANI-1 dataset result from normal mode sampling. Further details of the ANI-1 dataset can be found in the paper by Smith et al. 2017⁵³.

Fine-tuning is performed with a second dataset, the GDB7-20-TS dataset, which contains structures and energies of the critical points (reactant, TS, and product) of approximately 12k gas phase elementary organic reactions⁶⁴. The GDB7-20-TS dataset is computed at the ω B97X-D3/def2-TZVP level of theory. We re-optimize all structures and re-compute potential energies at the ω B97X/6-31G(d) level of theory. If a reactant, product, or TS fails the re-optimization, all structures associated with the reaction are removed from the test set. Details and criteria for validating critical point structures can be found

in Section II E. The final set of reaction structures is the fine-tuning set for this work.

B. GNN Potential Energy Functions

GNNs are a subset of neural networks that have had significant success within computational chemistry. To compose a graph let $G = (V, E)$ denote a graph with node attributes X_v for $v \in V$. Given a set of graphs $\{G_1, \dots, G_N\} \subseteq \mathcal{G}$ and their respective labels $\{y_1, \dots, y_N\} \subseteq \mathcal{Y}$, the task of graph supervised learning is to learn a representation vector h_G that serves to predict the label of an entire graph, $y_G = g(h_G)$. For material property prediction, G is a material graph, where nodes represent atoms. Proximal atoms are connected by edges, and the label is the property to be predicted, such as potential energy.

In this work, we use the SchNet model⁴⁷ which learns representation vectors h_v for every node $v \in \mathcal{G}$ through a general message passing scheme⁴⁵. In this strategy, the representation of a node is iteratively updated by aggregating the representations of its neighbors. After k iterations of aggregation, the representation vector $h_v^{(k)}$ captures the structural information within its k -hop network neighborhood. The SchNet model employs a continuous convolution filter to weight the aggregated neighbor representations by the pairwise distance between nodes. The k -th layer of SchNet is described by equation 1

$$h_v^{(k)} = \sum_{u \in \mathcal{N}(v)} h_u^k \cdot W^k(r_w - r_v) \quad (1)$$

where $h_v^{(k)}$ is the representation vector of node v at the k -th layer, $\mathcal{N}(v)$ is the set neighbors of v , and $h_v^{(0)} = X_v$. W^k is a filter generating network $W^l: \mathbb{R}^3 \rightarrow \mathbb{R}^F$ that maps from atomic positions r_w and r_v to a value in the corresponding filter bank, weighting the message based on neighbor distance. The total energy of a molecule is calculated as a sum of predictions of atomic contributions from vector representations from the final iteration K .

$$Energy = \sum_{N_{atoms}} MLP(h_v^K) \quad (2)$$

C. Training Details

We use the SchNet model included in Pytorch Geometric^{47,90}. To find optimal model hyperparameters we use Bayesian optimization as implemented in the Ax adaptive experimentation program^{91,92}. In Bayesian optimization minimum and maximum values for each hyperparameter of interest are defined. An ensemble of trial model trainings is performed, each with randomly sampled hyperparameter values within the pre-defined ranges. A GP is then fit to the hyperparameter-validation performance, mapping from hyperparameter values to validation performance. Once the initial GP model is trained, future trials are selected through the expected improvement acquisition function, which

TABLE I. Hyperparameter ranges of the SchNet model explored during Bayesian optimization and final value.

Hyperparameter	Range	Final Value
Hidden Channels	16-256	39
Number of Filters	16-256	111
Interaction Blocks	2-14	12
Number of Gaussians	16-128	105
Cutoff	2-12	8.0416
Learning Rate	$1^{-4} \cdot 2^{-3}$	2.94^{-4}
Batch Size	-	768

balances exploring areas of high-performance and areas of high uncertainty in hyperparameter space. A new set of trials with hyperparameters selected by the GP is performed, and the resulting hyperparameter-validation performance results are added to the GP model. This process is repeated until a user defined computational budget is reached. Further details of Bayesian Optimization, GP, and acquisition functions can be found in the paper by Snoek et al. 2012⁹¹.

In this work, 96 trials are performed, with each model being trained for 50 epochs on a 2080Ti GPU on the ANI-1 dataset. We use an 80/10/10 train/test/validation split. The hyperparameters and ranges explored are shown below in Table 1. Once all 96 trials are complete, we choose the best performing model as our final model. The hyperparameters are shown in Table I and validation mean absolute error (MAE) of the final model can be found in Section III A.

The best model, with hyperparameters shown in Table I, is then used for the fine-tuning on the GDB7-20-TS re-optimized to the ω B97X/6-31G(d) level of theory. The details of the fine-tuning dataset are provided in section II A. During the fine-tuning the model parameters are fixed, but a small grid search is performed over the learning rate and batch size. From the re-computed GDB7-20-TS dataset 300 reactions are randomly sampled and reserved as a training validation set. All models are allowed to train for 100 epochs. We evaluate each model on the validation sets of both the ANI-1 and Fine-Tuning sets. The model with the best performance on both validation sets is selected as the final model with which to perform FSM calculations.

D. Transition State Searches

We use the FSM with internal coordinates interpolation. The FSM produces an approximate reaction pathway from which a TS guess geometry can be taken. The approximate pathway takes a chain-of-states form, similar to that of the NEB and growing string method (GSM)^{17,18,27,80}. The chain-of-states consists of intermediate geometries along the reaction pathway, often referred to as nodes. The approximate reaction pathway is iteratively built up by alternately adding interior nodes to reactant and product sides of a growing string. The details of adding new nodes is shown in Figure 1 on the Müller-Brown test potential⁶. First, interpolation is per-

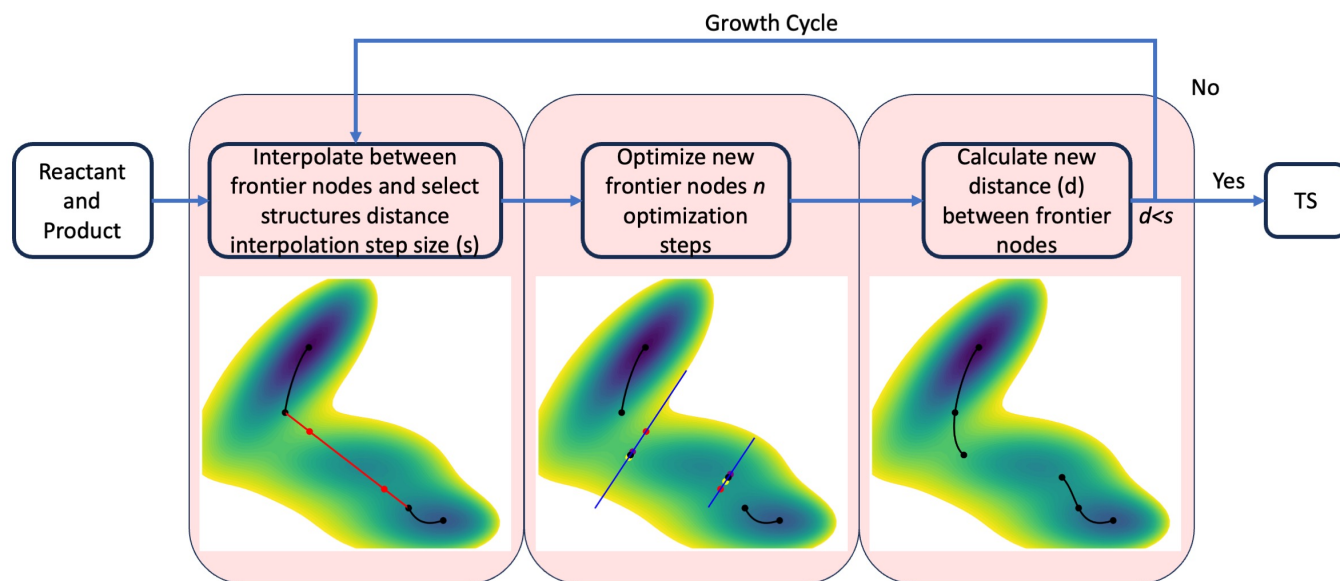


FIG. 1. Flow chart of the FSM with visualization of growth cycle steps on the Müller-Brown test potential. Interpolated paths and structures are shown in red, yellow is the node position after the first optimization cycle, purple shows the position after the second optimization cycle. Black nodes are in their final position (frozen).

formed between the current innermost (frontier) nodes of the growing string. The frontier nodes are converted to internal coordinates^{77,93,94} and linear interpolation is performed. This interpolation method generates smooth pathways of physically valid structures between endpoints²⁷. New reactant and product side structures are selected from the interpolated path based on a fixed step size s as shown in the leftmost image of Figure 1. The new frontier nodes are optimized on the hyperplane orthogonal to the current reaction path, ensuring the nodes lie close to the minimum energy pathway. All node optimizations are performed with L-BFGS-B optimization^{95,96} with backtracking linesearches. After all optimization steps are taken the geometries are frozen and will not change for the remainder of the calculation. This process is repeated until the reactant and product side strings meet. The highest energy node from the unified string is taken as the TS guess geometry and is refined to the exact TS via a local surface walking optimization algorithm. In-depth information on the effects of internal coordinates interpolation, comparison node optimization algorithms, and the effects of other user input parameters is presented in Marks & Gomes 2024²⁷.

Four TS searches are performed and validated for each reaction in the test set. Two TS searches are performed entirely with *ab-initio* potentials, one with a large step size and one with a small step size. The small step size parameters are a minimum number of 18 nodes, maximum linesearch steps 3, and maximum optimization steps 1. These parameters are found to have the highest success rate across chemically diverse benchmark sets. The large step size parameters are

the set of parameters found to most efficiently produce high-quality TS guesses without significantly compromising success rate²⁷. The large step size parameters are identical with the exception of the minimum number of nodes, which is reduced to nine, doubling the interpolation step size.

Each TS search occur in two major steps: the FSM,^{18,27} which provides the TS guess geometry, and the local surface-walking algorithm⁵ that refines the guess to the exact TS. We calculate the cost of a TS search as the sum of the DFT calculations required by the FSM and local surface walking algorithm. When performing the FSM with a GNN potential energy function, it is assumed that it has negligible cost, as gradient calculations of neural networks are orders of magnitude less computationally expensive than *ab-initio* calculations^{43,45}. As a result, when the FSM is performed with a GNN PES the entire cost of the TS search is incurred during the local surface walking algorithm. Additional computational cost is incurred during the validation of the TS, specifically in the intrinsic reaction coordinate (IRC) calculation and production of reactant/product structures. However, the cost of these calculations is unique to their starting point/chemical system and is not a reflection of the algorithm/PES used in this work.

The two remaining TS searches occur with the small step size parameters using a pre-trained GNN potential energy function for the FSM portion of the TS search. One search is done with the model resulting from training on the ANI-1 dataset (GNN-ANI1). The other search is performed with the GNN potential energy functions trained on the ANI-1 dataset

and fine-tuned (GNN-FT) on the GDB7-20-TS⁶⁴.

E. Computational Details

All electronic structure calculations in this work are performed at the ω B97X⁹⁷/6-31G(d)⁹⁸ level of theory using QChem 6⁹⁹. The ω B97X xc functional is classified as a range-separated hybrid generalized gradient approximation (GGA) functional^{98–105}. The ANI-1 dataset is calculated and published at the ω B97X/6-31G(d) level of theory and accounts for the vast majority of the electronic structure calculations used in this work. Re-computing the fine-tuning set and performing TS searches at the ω B97X/6-31G(d) level of theory has negligible cost compared to the cost of re-optimizing ANI-1 to a more favorable level of theory. As a result, all electronic structure calculations in this work are performed at the ω B97X/6-31G(d) level of theory. The barrier height and reaction energy errors associated with the ω B97X/6-31G(d) level of theory are not ideal for applying the pre-trained models produced in this work; however, this work is intended to be a proof of concept for introducing ML PES-driven TS searches.

TS guesses were refined to the exact TS using the partitioned rational function optimization (P-RFO) method^{2,5} in QChem. TS were validated using vibrational frequency calculations and the IRC method implemented in QChem. In some cases (ex. the alanine dipeptide system) the IRC calculation terminates before reaching the reactant and/or product structures. This is due to areas of relatively flat gradient that satisfies the convergence criteria of the IRC. The convergence criteria of traditional geometry optimizations (used to obtain initial reactant/product structures) is tighter and uses a different algorithm to take steps. Therefore, when an IRC calculation terminates before reaching reactant/product structures, the end structures of the IRC calculation are input to geometry optimizations in QChem. The final structures from the geometry optimizations are compared to the reactant and product. The energies of each step in the geometry optimization are examined to ensure a smooth decrease of energy, indicating no energetic barriers.

Vibrational frequency calculations are used to validate all critical points. TS must have exactly one imaginary frequency. In all test reactions, except the alanine dipeptide system, the imaginary frequencies significantly exceed -200cm^{-1} as shown in Table III. This corresponds to significant decrease in energy when moving forward or backward along the coordinate associated with that eigenvalue of the Hessian matrix. More than one imaginary frequency indicates decreases in energy along multiple coordinates, suggesting that the position is not a first-order saddle point. For reactants and products the rational function optimization algorithm^{2,5} implemented in QChem is used to perform geometry optimizations, which are similarly validated by vibrational frequency analysis. Minima (reactants/products) must have no imaginary frequencies.

III. MACHINE LEARNING RESULTS

A. Pre-training Results

The best model (GNN-ANI1) from the Bayesian Optimization described in Section II C is taken as the final model. On the ANI-1 dataset the model achieves a validation RMSE of 1.4 kcal/mol, which is under the established limit for chemical accuracy.

To evaluate the performance of the GNN-ANI1 we take the reactants, TS, and products of the benchmark set of reactions shown in Table III and predict the potential energies of each structure. In Table II structures are grouped by chemical phenomena present in the system. The GNN-ANI1 model does not achieve chemical accuracy across any of the splits of the structures despite its validation performance on the ANI-1 dataset.

Reactants and products exist as energetic minima, an area of chemical space well described by the ANI-1 dataset. However, the GNN-ANI1 model shows an error of 19.4 kcal/mol. This is largely due to the presence of non-covalent interactions in reactant/product structures of the ethane dehydrogenation reaction, the formaldehyde decomposition reaction, and the Diels-Alder reaction. Non-covalent interactions and H-H covalent bonds are not present in the ANI-1 dataset and introduce a large degree of error into prediction of systems with these chemical phenomena present. This is more easily observed when the minima are grouped by the presence of more than one molecule in the system. On unimolecular reactants and products the GNN-ANI1 has an error of 4.1 kcal/mol, significantly lower than the average across the set.

The poor performance in predicting TS structure potential energies is expected given the data distribution of the ANI-1 dataset. The area of chemical space associated with TS geometries of bond breaking/formation lies far from the local minima well described by the ANI-1 set. Despite the high error of the GNN-ANI1 model we perform TS searches across the benchmark set, using it as the potential for the FSM. The results of these searches can be found in Section IV A.

B. Fine-Tuning Results

To improve the models' ability to describe non-covalent interactions and areas of chemical space outside local minima we perform fine-tuning on the GDB7-20-TS dataset re-optimized to the ω B97X/6-31G(d) level of theory. Details of the dataset and re-optimization can be found in Section II A.

The effects of fine-tuning are quantified by predicting the potential energy of the same set of benchmark structures shown in Table II. The fine-tuning improves the model across all categories. Fine-tuning reduces the model prediction error of reactant and product energies from 19.4kcal/mol to 1.3kcal/mol. When splitting the reaction set by the presence of more than one molecule, it is clear that the fine-tuning allows the model to better describe energetics associated with non-covalent interactions. The error associated with predicting the energies of unimolecular systems is reduced from 4.1kcal/mol

TABLE II. Error of GNN-ANI1 and GNN-FT models relative to ω B97X/6-31G(d) on reactants, products and transition states from the validation set of reactions.

Set of Structures	GNN-ANI1 Error kcal/mol	GNN-FT Error kcal/mol	Percent Reduction
All Reactants and Products	19.4	1.3	93.49
All Transition States	124.3	76.9	38.14
Bi-molecular Reaction Transition States	249.2	147.6	40.75
Unimolecular Reaction Transition States	30.7	23.9	22.19
Unimolecular Minima	4.1	1.6	61.48
Bi-molecular structures (Reactant/Product)	78.8	0.9	98.8

to 1.6, the smallest absolute reduction in error observed. In contrast, the error associated with bimolecular minima structures is reduced from 78.8kcal/mol to 0.9kcal/mol, a 98.8% reduction in error.

Overall, the fine-tuning lowers the error of the GNN from 124.3kcal/mol to 76.9kcal/mol, a significant reduction. However, a large portion of this reduction is likely due to the learning of non-covalent interactions discussed above. When making predictions about TS of reactions with non-covalent interactions we see reduction in average error from 249.2 to 147.6kcal/mol, a 40.75% reduction. However, with reactions where no non-covalent interactions are present, the error is only reduced by 22.19%, the smallest percent reduction of any category.

The results in Table II indicates that the fine-tuning significantly reduces the error in our GNN. This reduction in error is largely due to the model learning non-covalent interactions. However, the model fails to make a significant reduction in error in the area of chemical space associated with TS phenomena (bond dissociation, formation, compression/stretching). The GNN-FT model is chemically accurate for minima structures regardless of the presence of non-covalent interactions. Despite the improvements from fine-tuning, the GNN-FT model is not chemically accurate across all relevant areas of chemical space and has a high degree of error around TS. More configurationally diverse quantum chemistry datasets are required to resolve this issue, as fine-tuning is not sufficient.

IV. TRANSITION STATE SEARCHES

A. Benchmark Set Results

Automated TS searches occur in two major steps. In the first step, a non-local path-finding algorithm explores the PES between reactant and product configurations and outputs a guess of the TS geometry^{17,18,25,26}. In the second step, the TS geometry is refined to the exact TS using a local surface walking algorithm^{5,25}. The focus of this work is incorporation of GNN potential energy functions into the non-local path-finding algorithm. Details of the calculations can be found in Sections 2.4 and 2.5.

Our test set, shown in Table III, is comprised of well studied chemical reactions that are commonly used as test/benchmark cases in TS search literature^{80,106-109}. This test set contains

diverse reaction phenomena including isomerization, ring formation/opening, and bond dissociation/formation. First TS searches are performed on each reaction using DFT, giving a reference TS at the ω B97X/6-31G(d) level of theory and a baseline computational cost. DFT based searches successfully find a TS for each reaction that agrees with literature values and is validated by vibrational frequency¹¹⁰ and IRC calculations. Next, we perform TS searches using the GNN-ANI1 PES for the FSM. When performing the FSM on the GNN-ANI1 model only five of the seven calculations yield a TS guess geometry that converges to a saddle point when input to the P-RFO. In the formaldehyde decomposition and ethane dehydrogenation reactions the guess geometry resulting from the GNN-ANI1 FSM either fail to converge to a point of zero first order gradient (ethane dehydrogenation) or converge to a local minima structure (formaldehyde decomposition). Both of these modes of failure occur when a guess geometry is outside the basin of attraction of the TS. The P-RFO algorithm attempts to maximize the eigenvalue of the Hessian matrix with the largest imaginary frequency while minimizing all other frequencies. When the P-RFO algorithm fails to converge to an area of zero first order gradient, it is generally due to a non-physical initial guess structure that lies far from any saddle point, as is the case in ethane dehydrogenation. The ethane dehydrogenation reaction is discussed in detail in Section IV B. In the case of formaldehyde decomposition the TS guess geometry has a smallest vibrational frequency of 227.43cm^{-1} which is reduced to -246.33cm^{-1} over 84 optimization steps. This is far from the reference imaginary frequency of -2050.11cm^{-1} obtained from the DFT TS search. Visual inspection of the structure and vibrational frequencies revealed that this is the dissociated H_2+CO state, with the imaginary frequency corresponding to rotation of the H_2 molecule from parallel to perpendicular to the CO molecule.

As DFT searches with identical parameters and starting structures are successful for both ethane dehydrogenation and formaldehyde decomposition, the failure is due to the change in PES used in the FSM. Additionally, the GNN-ANI1 model performs particularly poorly across all areas of chemical space for systems with non-covalent interactions and H-H interactions, both of which are present in ethane dehydrogenation and formaldehyde decomposition. In the five successful cases, TS searches using the GNN-ANI1 average 34.4 DFT calculations while traditional DFT searches average 77.2 DFT calculations. This shows that when successful, using GNN PES to perform the FSM significantly reduces the computational cost

of the TS search. However, when the entire test set is compared, including failed runs, the GNN-ANI1 searches average 72.28 DFT calculations while full DFT runs average 70.71 DFT calculations. This underscores the importance of reliable TS searches. Not only do failed searches not produce a TS, but they also require significant computational resources before failing. Resubmission of TS searches with new parameters would introduce further computational expenses.

TS searches with the GNN-FT PES for the FSM perform significantly better than FSM calculations with the GNN-ANI1 model. GNN-FT calculations converge to a first order saddle point in all searches. On average, GNN-FT-based TS searches require 37.4 DFT calculations to locate the exact TS while DFT searches with identical parameters require 70.71 DFT calculations on average. Relative to searches with the GNN-ANI1 PES, this is a 48.3% reduction in computational cost with an improved convergence rate, as six of the seven searches find the reference saddle point. The ethane dehydrogenation reaction search does not find the reference saddle point, instead converging to a different saddle point. The ethane dehydrogenation reaction is discussed further in Section IV B.

User-input parameters of the FSM play a large role in the cost and success of the TS search. In Table III, we perform TS searches with identical parameters, only varying the PES. This enables study of the effects of the PES on the success and cost of the overall TS search. However, the parameters used for the FSM calculations in Table 3 are considered expensive parameters; small interpolation steps are taken, resulting in a dense final string. This results in accurate but expensive TS guesses. In a high-throughput screen it is much more realistic to use parameters that offer a balance between reliability and cost. We perform DFT-TS searches on our test set with twice the interpolation step size and compare the cost of these searches to the original GNN-FT searches in Figure 2.

As accuracy should be prioritized when selecting parameters, we do not perform new GNN-FT TS searches with the larger interpolation step size as the computational cost of the FSM is effectively negligible when performed with the GNN-FT PES. The more efficient parameters for the DFT searches results in a significant reduction in DFT calculations. The optimized DFT TS searches require 45.71 DFT calculations on average, a 35.4% reduction compared to the results presented in Table III. The reduction in computational cost reduces the reliability of the TS search due to the coarser approximate reaction path. The full DFT search for the TS of the ethane dehydrogenation fails to converge to any saddle point, as denoted by the asterisk in Figure 4. Even with computationally efficient parameters full DFT TS searches are unable to outperform TS searches using the GNN-FT potential for the FSM while still achieving similar reliability.

B. Ethane Dehydrogenation

Ethane dehydrogenation has been demonstrated in the current work and prior literature⁸⁰ to be a difficult test case for FSM based TS searches to identify the saddle point of interest.

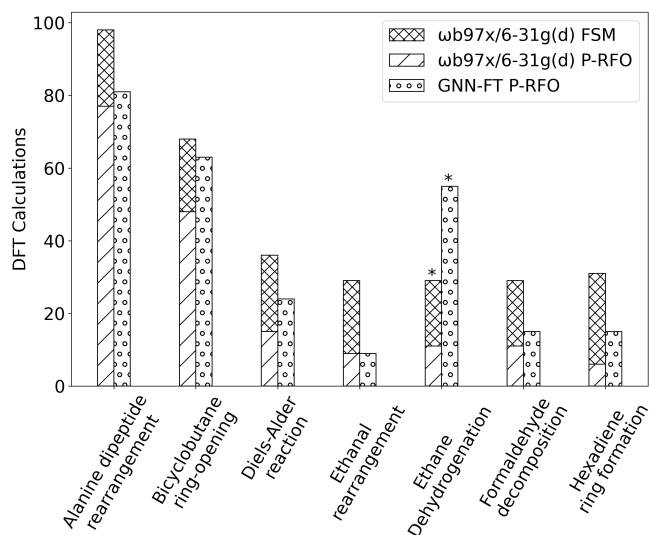


FIG. 2. DFT calculations to converge to the exact TS of the test set. TS searches using the GNN-FT potential during the FSM are shown in blue are performed with Minimum Nodes 18 Maximum linesearch steps 3 maximum optimization steps 1. ω B97X/6-31G(d) TS searches are performed with Minimum Nodes 9 Maximum linesearch steps 3 maximum optimization steps 1.

When performing the FSM calculation with the GNN-ANI1 PES, a TS guess geometry exhibiting no imaginary transition mode is obtained. The P-RFO TS refinement calculation is initialized with a geometry lacking the proper Hessian structure, and the calculation is terminated after 250 geometry optimization steps without the identification of a saddle point resulting in a failed TS search.

A potential energy reaction coordinate diagram of approximate reaction pathways calculated by the GNN-FT and DFT FSM is shown in Figure 3. When performing the FSM with the GNN-FT PES, a TS guess geometry with an initial imaginary frequency of -1200.39cm^{-1} is obtained. This guess geometry exhibits a significantly lower potential energy barrier for the reaction than the reference DFT TS and barrier, shown in Figure 3A. The potential energy of the GNN-FT FSM string and reference DFT FSM string are plotted as a function of path arc length in Figure 3A. When input to the P-RFO algorithm in QChem the GNN-FT TS guess geometry converges to a saddle point structure with an imaginary frequency of -1570.00cm^{-1} , which is shown in red brackets in Figure 3C. This differs significantly from the DFT-based calculation, which gives a guess with an imaginary frequency of -1850.06cm^{-1} . This converges to the structure shown in green brackets in Figure 3B, which has an imaginary frequency of -2382.57cm^{-1} . Geometrically the two transition states are exceedingly similar. To validate the nature of each saddle point, IRC calculations were performed using the two saddle points as starting points. The resulting minimum energy pathway (MEP) are shown in Figure 3B and 3C. In Figure 3B it is clear that this is the correct TS for the ethane dehydrogenation reaction. One end of the path ends at the reactant structure while the other ends at the product structure. In Figure

TABLE III. Thermodynamic parameters of each reaction in the test set and DFT calculations required to locate the exact transition state when performing the FSM with GNN-ANI1, GNN-FT, and ω B97X/6-31G(d) potential energy functions.

Reaction	ΔH_{rxn} kcal/mol	Activation Energy kcal/mol	GNN-ANI1 DFT Calculations	GNN-FT DFT Calculations	Full DFT	Reference Imaginary Frequency cm^{-1}
Alanine dipeptide rearrangement	1.1	6.6	57	81	118	-48.62
Bicyclobutane ring-opening	-16.5	22.0	47	63	105	-304.54
Diels-Alder reaction	-51.5	73.58	49	24	60	-659.26
Ethanal rearrangement	-16.0	59.0	7	9	48	-2307.15
Ethane dehydrogenation	47.0	135.2	250 ^a	55 ^b	59	-2382.57
Formaldehyde decomposition	10.4	95.9	84 ^c	15	50	-2050.11
Hexadiene ring formation	4.8	55.62	12	15	55	-722.73

^a Reached maximum optimization cycles in P-RFO saddle point search

^b Converged to incorrect saddle point

^c Converged to local minimum

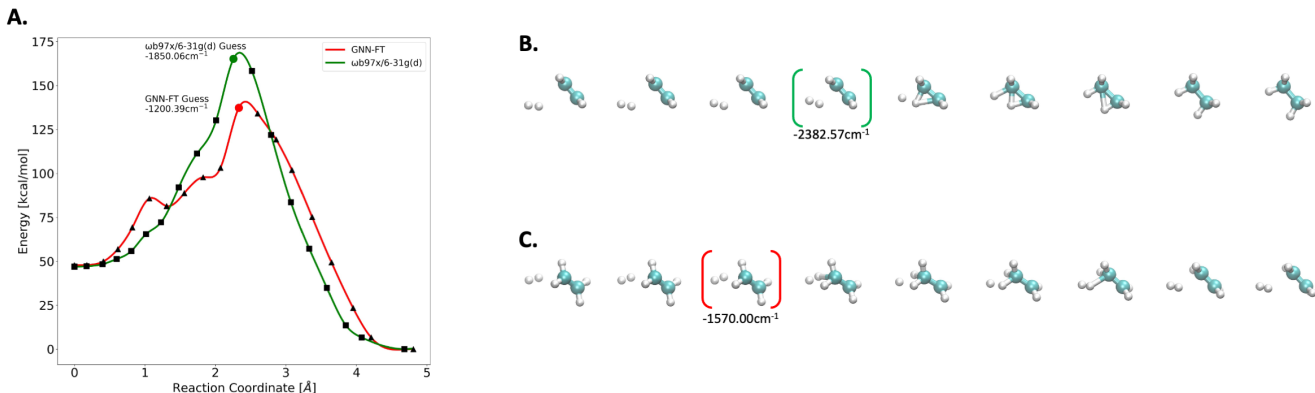


FIG. 3. A. Energy vs arc length along FSM paths of the Ethane Dehydrogenation reaction. Note that energies are calculated with the respective model. B. MEP resulting from IRC calculation started with transition state from ω B97X/6-31G(d) based search. C. MEP resulting from IRC calculation started with transition state obtained from SchNet-based search.

3C the first-order saddle point obtained from the GNN-FT FSM corresponds to an entirely different reaction: a hydrogen exchange reaction on ethene. This indicates that the largest imaginary frequency of the TS guess given by the GNN-FT FSM corresponds to the hydrogen exchange reaction, not the dehydrogenation reaction.

C. Alanine Dipeptide

Previous studies of the alanine dipeptide rearrangement reaction have examined the location of minimum energy structures (Ref. Mironov *et al.*¹¹¹ and references therein), the minimum energy pathways of structural transitions^{17,24,25}, and the minimum free energy transition pathways¹¹². The alanine dipeptide exhibits multiple conformational minimum energy structures with well-characterized, relatively low transition barriers. It serves as a representative model of protein dynamics, making it an important test case for reaction path finding algorithms. This isomerization reaction involves the rotation about the ϕ (C-N-C $_{\alpha}$ -C) and ψ (N-C-C $_{\alpha}$ -N) Ramachadran dihedral angles, shown in Figure 4a. In Figure 4b, the minimum energy pathway computed at the ω B97X/6-31G(d) level of theory is projected onto the Ramachadran angles together with

the approximate reaction pathways computed by the GNN-FT FSM and DFT FSM. The GNN-FT and DFT FSM calculations use identical hyperparameters and qualitatively produce similar pathways. The ϕ and ψ dihedral coordinates along the GNN-FT and DFT FSM pathways are rotated in a single concerted step while the true minimum energy pathway shows a step-wise rotation of one dihedral coordinate followed by the other. The similarity of FSM pathways and close proximity of TS guesses indicates that the GNN-FT potential performs comparably to the DFT potential in this case. Ultimately, both GNN-FT and DFT TS guesses converge to the exact TS geometry when further refined.

V. CONCLUSION

In this work, we demonstrate that the incorporation of ML-based PES into the FSM TS search algorithm significantly reduces the computational cost associated with DFT calculations required for TS searches by nearly 50% while maintaining a high success rate. This work shows that with appropriate training, ML PES representations are suitable for incorporation into TS searches and other routine computational chemistry tasks. We assess the accuracy and success

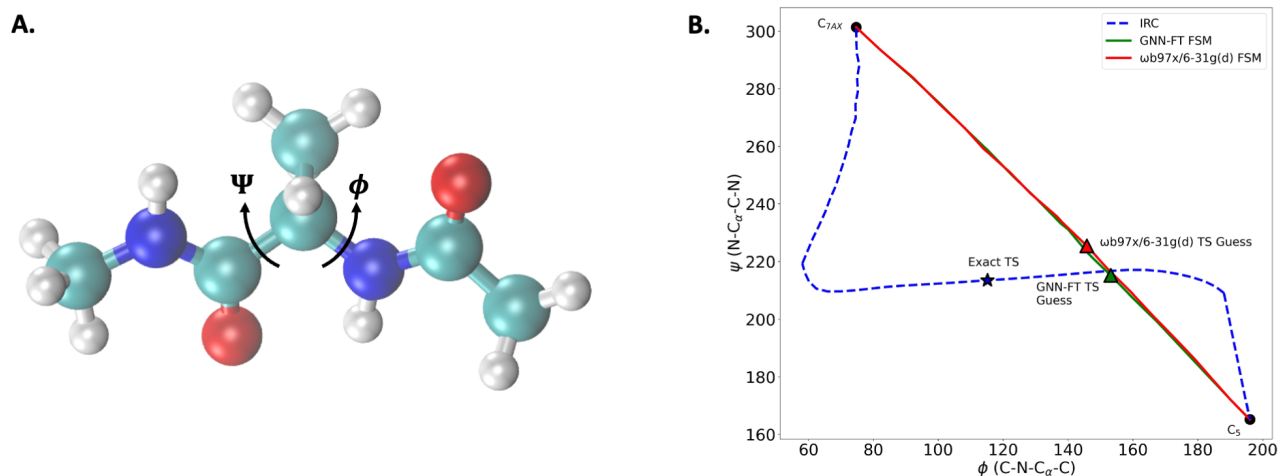


FIG. 4. A. C₅ conformer of the alanine dipeptide system with Ramachandran angles labeled. B. Ramachandran angles of the alanine dipeptide system along pathways taken by IRC, GNN-FT FSM, and ω B97X/6-31G(d) FSM.

rate of our approach based on a benchmark suite of several well-studied organic chemical reaction. In each test case, we successfully identify TS saddle point structures in fewer DFT calculations compared to the traditional approach, and in all but one case, identify the intended TS structure connecting original reactant and product structures. We show how fine-tuning our ML-based PES on approximately 11K TS structures greatly improves model accuracy along reaction pathways, which ultimately leads to the success of the ML-based TS search algorithms. The reduction in computational cost can enable the use of such tools for the high-throughput study of reaction mechanisms and complete mapping of complex reaction networks. The incorporation of improved molecular representation learning algorithms^{49,50,113}, as well as datasets of configurationally diverse electronic structure calculations, is essential for further improvement of this work.

ACKNOWLEDGMENTS

J.G acknowledges start up funding from The University of Iowa. This research was supported in part through computational resources provided by The University of Iowa.

DATA AVAILABILITY STATEMENT

The data that support the findings of this study are openly available in Zenodo at <https://doi.org/10.5281/zenodo.14629429>, reference number 14629429.

¹C. J. Cerjan and W. H. Miller, The Journal of Chemical Physics **75**, 2800 (1981).

²A. Banerjee, N. Adams, J. Simons, and R. Shepard, The Journal of Physical Chemistry **89**, 52 (1985).

³J. Baker, Journal of Computational Chemistry **7**, 385 (1986).

⁴D. J. Wales, Journal of the Chemical Society, Faraday Transactions **89**, 1305 (1993).

⁵A. Heyden, A. T. Bell, and F. J. Keil, The Journal of chemical physics **123**, 224101 (2005).

⁶K. Müller and L. D. Brown, Theoretica chimica acta **53**, 75 (1979).

⁷R. Elber and M. Karplus, Chemical Physics Letters **139**, 375 (1987).

⁸P. Y. Ayala and H. B. Schlegel, The Journal of Chemical Physics **107**, 375 (1997).

⁹E. Weinan, W. Ren, and E. Vanden-Eijnden, Physical Review B **66**, 052301 (2002).

¹⁰S. A. Trygubenko and D. J. Wales, The Journal of chemical physics **120**, 2082 (2004).

¹¹E. L. Kolsbjerg, M. N. Groves, and B. Hammer, The Journal of Chemical Physics **145**, 094107 (2016).

¹²J.-W. Chu, B. L. Trout, and B. R. Brooks, The Journal of Chemical Physics **119**, 12708 (2003).

¹³G. Henkelman and H. Jónsson, The Journal of chemical physics **113**, 9978 (2000).

¹⁴G. Henkelman, B. P. Uberuaga, and H. Jónsson, The Journal of chemical physics **113**, 9901 (2000).

¹⁵P. Maragakis, S. A. Andreev, Y. Brumer, D. R. Reichman, and E. Kaxiras, The Journal of Chemical Physics **117**, 4651 (2002).

¹⁶A. W. Ruttinger, D. Sharma, and P. Clancy, Journal of Chemical Theory and Computation **18**, 2993 (2022).

¹⁷B. Peters, A. Heyden, A. T. Bell, and A. Chakraborty, The Journal of chemical physics **120**, 7877 (2004).

¹⁸A. Behn, P. M. Zimmerman, A. T. Bell, and M. Head-Gordon, The Journal of chemical physics **135**, 224108 (2011).

¹⁹W. Quapp, The Journal of Chemical Physics **122**, 174106 (2005).

²⁰P. Zimmerman, Journal of Chemical Theory and Computation **9**, 3043 (2013).

²¹P. M. Zimmerman, Journal of Computational Chemistry **36**, 601 (2015).

²²M. Jafari and P. M. Zimmerman, Journal of Computational Chemistry **38**, 645 (2017).

²³Y. V. Suleimanov and W. H. Green, Journal of Chemical Theory and Computation **11**, 4248 (2015).

²⁴A. Behn, P. M. Zimmerman, A. T. Bell, and M. Head-Gordon, Journal of Chemical Theory and Computation **7**, 4019 (2011).

²⁵S. M. Sharada, P. M. Zimmerman, A. T. Bell, and M. Head-Gordon, Journal of chemical theory and computation **8**, 5166 (2012).

²⁶P. M. Zimmerman, The Journal of chemical physics **138**, 184102 (2013).

²⁷J. Marks and J. Gomes, arXiv preprint arXiv:2407.09763 (2024).

²⁸J. Behler and M. Parrinello, Physical review letters **98**, 146401 (2007).

- ²⁹S. Chmiela, H. E. Sauceda, K.-R. Müller, and A. Tkatchenko, *Nature communications* **9**, 3887 (2018).
- ³⁰L. Zhang, J. Han, H. Wang, R. Car, and W. E, *Physical review letters* **120**, 143001 (2018).
- ³¹B. Anderson, T. S. Hy, and R. Kondor, *Advances in neural information processing systems* **32** (2019).
- ³²C. W. Park, M. Kornbluth, J. Vandermause, C. Wolverton, B. Kozinsky, and J. P. Mailoa, *npj Computational Materials* **7**, 73 (2021).
- ³³C. Casewit, K. Colwell, and A. Rappe, *Journal of the American Chemical Society* **114**, 10035 (1992).
- ³⁴J. J. Stewart, *Journal of Molecular Modeling* **13**, 1173 (2007).
- ³⁵A. C. Van Duin, S. Dasgupta, F. Lorant, and W. A. Goddard, *The Journal of Physical Chemistry A* **105**, 9396 (2001).
- ³⁶D. W. Brenner, O. A. Shenderova, J. A. Harrison, S. J. Stuart, B. Ni, and S. B. Sinnott, *Journal of Physics: Condensed Matter* **14**, 783 (2002).
- ³⁷J. J. Winetrou, K. Kanhaiya, J. Kempainen, P. J. in 't Veld, G. Sachdeva, R. Pandey, B. Damirchi, A. van Duin, G. M. Odegard, and H. Heinz, *Nature Communications* **15** (2024), 10.1038/s41467-024-50793-0.
- ³⁸A. Goodrow, A. T. Bell, and M. Head-Gordon, *The Journal of chemical physics* **129**, 174109 (2008).
- ³⁹A. Goodrow, A. T. Bell, and M. Head-Gordon, *The Journal of Chemical Physics* **130**, 244108 (2009).
- ⁴⁰A. Goodrow, A. T. Bell, and M. Head-Gordon, *Chemical Physics Letters* **484**, 392 (2010).
- ⁴¹T. B. Blank, S. D. Brown, A. W. Calhoun, and D. J. Doren, *The Journal of chemical physics* **103**, 4129 (1995).
- ⁴²C. M. Handley, G. I. Hawe, D. B. Kell, and P. L. Popelier, *Physical Chemistry Chemical Physics* **11**, 6365 (2009).
- ⁴³J. S. Smith, O. Isayev, and A. E. Roitberg, *Chemical Science* **8**, 3192 (2017).
- ⁴⁴J. S. Smith, B. T. Nebgen, R. Zubatyuk, N. Lubbers, C. Devereux, K. Barros, S. Tretiak, O. Isayev, and A. E. Roitberg, *Nature communications* **10**, 2903 (2019).
- ⁴⁵J. Gilmer, S. S. Schoenholz, P. F. Riley, O. Vinyals, and G. E. Dahl, in *International conference on machine learning* (PMLR, 2017) pp. 1263–1272.
- ⁴⁶K. T. Schütt, F. Arbabzadah, S. Chmiela, K. R. Müller, and A. Tkatchenko, *Nature communications* **8**, 13890 (2017).
- ⁴⁷K. T. Schütt, H. E. Sauceda, P.-J. Kindermans, A. Tkatchenko, and K.-R. Müller, *The Journal of Chemical Physics* **148**, 241722 (2018).
- ⁴⁸O. T. Unke and M. Meuwly, *Journal of chemical theory and computation* **15**, 3678 (2019).
- ⁴⁹J. Gasteiger, J. Groß, and S. Günnemann, *arXiv preprint arXiv:2003.03123* (2020).
- ⁵⁰S. Batzner, A. Musaelian, L. Sun, M. Geiger, J. P. Mailoa, M. Kornbluth, N. Molinari, T. E. Smidt, and B. Kozinsky, *Nature communications* **13**, 2453 (2022).
- ⁵¹A. Musaelian, S. Batzner, A. Johansson, L. Sun, C. J. Owen, M. Kornbluth, and B. Kozinsky, *Nature Communications* **14**, 579 (2023).
- ⁵²R. Ramakrishnan, P. O. Dral, M. Rupp, and O. A. V. Lilienfeld, *Scientific data* **1**, 1 (2014).
- ⁵³J. S. Smith, O. Isayev, and A. E. Roitberg, *Scientific data* **4**, 1 (2017).
- ⁵⁴F. Noé, A. Tkatchenko, K.-R. Müller, and C. Clementi, *Annual review of physical chemistry* **71**, 361 (2020).
- ⁵⁵N. V. Tkachenko, A. A. Tkachenko, B. Nebgen, S. Tretiak, and A. I. Boldyrev, *Physical Chemistry Chemical Physics* **25**, 21173 (2023).
- ⁵⁶M. Kulichenko, J. S. Smith, B. Nebgen, Y. W. Li, N. Fedik, A. I. Boldyrev, N. Lubbers, K. Barros, and S. Tretiak, *The Journal of Physical Chemistry Letters* **12**, 6227 (2021).
- ⁵⁷J. Lan, A. Palizhati, M. Shuaibi, B. M. Wood, B. Wander, A. Das, M. Uytendaele, C. L. Zitnick, and Z. W. Ulissi, *npj Computational Materials* **9**, 172 (2023).
- ⁵⁸M. Schreiner, A. Bhowmik, T. Vegge, J. Busk, and O. Winther, *Scientific Data* **9**, 779 (2022).
- ⁵⁹S. Zhang, M. Z. Makoś, R. B. Jadrach, E. Kraka, K. Barros, B. T. Nebgen, S. Tretiak, O. Isayev, N. Lubbers, R. A. Messerly, *et al.*, *Nature Chemistry* **16**, 727 (2024).
- ⁶⁰J. S. Smith, B. Nebgen, N. Lubbers, O. Isayev, and A. E. Roitberg, *The Journal of chemical physics* **148** (2018).
- ⁶¹J. Vandermause, S. B. Torrisi, S. Batzner, Y. Xie, L. Sun, A. M. Kolpak, and B. Kozinsky, *npj Computational Materials* **6**, 20 (2020).
- ⁶²J. S. Smith, B. Nebgen, N. Mathew, J. Chen, N. Lubbers, L. Burakovsky, S. Tretiak, H. A. Nam, T. Germann, S. Fensin, *et al.*, *Nature communications* **12**, 1257 (2021).
- ⁶³M. Kulichenko, K. Barros, N. Lubbers, Y. W. Li, R. Messerly, S. Tretiak, J. S. Smith, and B. Nebgen, *Nature Computational Science* **3**, 230 (2023).
- ⁶⁴C. A. Grambow, L. Pattanaik, and W. H. Green, *Scientific data* **7**, 1 (2020).
- ⁶⁵P. van Gerwen, K. R. Briling, C. Bunne, V. R. Somnath, R. Laplaza, A. Krause, and C. Corminboeuf, *Journal of Chemical Information and Modeling* (2024).
- ⁶⁶K. A. Spiekermann, L. Pattanaik, and W. H. Green, *The Journal of Physical Chemistry* **126**, 3976 (2022).
- ⁶⁷S. Heinen, G. F. von Rudorff, and O. A. von Lilienfeld, *The Journal of Chemical Physics* **155**, 064105 (2021).
- ⁶⁸C. A. Grambow, L. Pattanaik, and W. H. Green, *The journal of physical chemistry letters* **11**, 2992 (2020).
- ⁶⁹M. Z. Makos, N. Verma, and E. C. Larson, *The Journal of Chemical Physics*, 024116 (2021).
- ⁷⁰R. Jackson, W. Zhang, and J. Pearson, *Chemical Science* **12**, 10022 (2021).
- ⁷¹L. Pattanaik, J. B. Ingraham, C. A. Grambow, and W. H. Green, *Physical Chemistry Chemical Physics* **22**, 23618 (2020).
- ⁷²S. Stocker, G. Csanyi, K. Reuter, and J. T. Margraf, *Nature communications* **11**, 5505 (2020).
- ⁷³M. Meuwly, *Chemical Reviews* **121**, 10218 (2021).
- ⁷⁴P. van Gerwen, A. Fabrizio, M. D. Wodrich, and C. Corminboeuf, *Machine Learning: Science and Technology* **3**, 045005 (2022).
- ⁷⁵E. Heid and W. H. Green, *Journal of Chemical Information and Modeling* **62**, 2101 (2021).
- ⁷⁶J. Baker, *Journal of computational chemistry* **8**, 563 (1987).
- ⁷⁷C. Peng, P. Y. Ayala, H. B. Schlegel, and M. J. Frisch, *Journal of Computational Chemistry* **17**, 49 (1996).
- ⁷⁸J. M. Bofill, *Journal of Computational Chemistry* **15**, 1 (1994).
- ⁷⁹G. Henkelman and H. Jónsson, *The Journal of Chemical Physics* **111**, 7010 (1999).
- ⁸⁰S. M. Sharada, P. M. Zimmerman, A. T. Bell, and M. Head-Gordon, *Journal of Chemical Theory and Computation* **8**, 5166 (2012).
- ⁸¹H. B. Schlegel, *Journal of Computational Chemistry* **3**, 214 (1982).
- ⁸²A. P. Bartók, M. C. Payne, R. Kondor, and G. Csányi, *Physical review letters* **104**, 136403 (2010).
- ⁸³A. Denzel, B. Haasdonk, and J. Kästner, *The Journal of Physical Chemistry A* **123**, 9600 (2019).
- ⁸⁴A. Denzel and J. Kästner, *Journal of Chemical Theory and Computation* **16**, 5083 (2020).
- ⁸⁵Y. Xie, J. Vandermause, L. Sun, A. Cepellotti, and B. Kozinsky, *npj Computational Materials* **7**, 40 (2021).
- ⁸⁶M. Schreiner, A. Bhowmik, T. Vegge, P. B. Jørgensen, and O. Winther, *Machine Learning: Science and Technology* **3**, 045022 (2022).
- ⁸⁷B. Wander, M. Shuaibi, J. R. Kitchin, Z. W. Ulissi, and C. L. Zitnick, *arXiv preprint arXiv:2405.02078* (2024).
- ⁸⁸T. Fink, H. Bruggesser, and J.-L. Reymond, *Angewandte Chemie International Edition* **44**, 1504 (2005).
- ⁸⁹T. Fink and J.-L. Reymond, *Journal of chemical information and modeling* **47**, 342 (2007).
- ⁹⁰M. Fey and J. E. Lenssen, *arXiv preprint arXiv:1903.02428* (2019).
- ⁹¹J. Snoek, H. Larochelle, and R. P. Adams, *Advances in neural information processing systems* **25** (2012).
- ⁹²E. Bakshy, L. Dworkin, B. Karrer, K. Kashin, B. Letham, A. Murthy, and S. Singh (2018) pp. 1–8.
- ⁹³W. Lee-Ping and C. Song, *The Journal of Chemical Physics* **144** (2016).
- ⁹⁴V. Bakken and T. Helgaker, *The Journal of Chemical Physics* **117**, 9160 (2002).
- ⁹⁵C. Zhu, R. H. Byrd, P. Lu, and J. Nocedal, *ACM Transactions on mathematical software (TOMS)* **23**, 550 (1997).
- ⁹⁶R. H. Byrd, P. Lu, J. Nocedal, and C. Zhu, *SIAM Journal on Scientific Computing* **16**, 1190 (1995).
- ⁹⁷J.-D. Chai and M. Head-Gordon, *The Journal of chemical physics* **128** (2008).

- ⁹⁸R. Ditchfield, W. J. Hehre, and J. A. Pople, *The Journal of Chemical Physics* **54**, 724 (1971).
- ⁹⁹E. Epifanovsky, A. T. Gilbert, X. Feng, J. Lee, Y. Mao, N. Mardirossian, P. Pokhilko, A. F. White, M. P. Coons, A. L. Dempwolff, *et al.*, *The Journal of chemical physics* **155**, 084801 (2021).
- ¹⁰⁰N. Mardirossian and M. Head-Gordon, *Physical Chemistry Chemical Physics* **16**, 9904 (2014).
- ¹⁰¹M. Bursch, J.-M. Mewes, A. Hansen, and S. Grimme, *Angewandte Chemie International Edition* **61**, e202205735 (2022).
- ¹⁰²K. S. Thanthiriwatte, E. G. Hohenstein, L. A. Burns, and C. D. Sherrill, *Journal of Chemical Theory and Computation* **7**, 88 (2011).
- ¹⁰³L. Goerigk and S. Grimme, *Physical Chemistry Chemical Physics* **13**, 6670 (2011).
- ¹⁰⁴Y. Shao, Z. Gan, E. Epifanovsky, A. T. B. Gilbert, M. Wormit, J. Kussmann, A. W. Lange, A. Behn, J. Deng, X. Feng, *et al.*, *Molecular Physics* **113**, 184 (2015).
- ¹⁰⁵F. Weigend and R. Ahlrichs, *Physical Chemistry Chemical Physics* **7**, 3297 (2005).
- ¹⁰⁶E. P. Blanchard Jr and A. Cairncross, *Journal of the American Chemical Society* **88**, 487 (1966).
- ¹⁰⁷G. Closs and P. Pfeffer, *Journal of the American Chemical Society* **90**, 2452 (1968).
- ¹⁰⁸M. J. Dewar and S. Kirschner, *Journal of the American Chemical Society* **97**, 2931 (1975).
- ¹⁰⁹P. B. Shevlin and M. L. McKee, *Journal of the American Chemical Society* **110**, 1666 (1988).
- ¹¹⁰E. B. Wilson, J. C. Decius, and P. C. Cross, *Molecular vibrations: the theory of infrared and Raman vibrational spectra* (Courier Corporation, 1980).
- ¹¹¹V. Mironov, Y. Alexeev, V. K. Mulligan, and D. G. Fedorov, *Journal of Computational Chemistry* **40**, 297 (2019).
- ¹¹²J. Vymetal and J. Vondrasek, *The Journal of Physical Chemistry B* **114**, 5632 (2010).
- ¹¹³N. Lubbers, J. S. Smith, and K. Barros, *The Journal of chemical physics* **148** (2018).
- ¹¹⁴M. Rupp, A. Tkatchenko, K.-R. Muller, and O. A. V. Lilienfeld, *Physical review letters* **108**, 058301 (2012).
- ¹¹⁵L. Blum and J.-L. Reymond, *Journal of the American Chemical Society* **131**, 8732 (2009).
- ¹¹⁶D. F. Brown, M. N. Gibbs, and D. C. Clary, *The journal of chemical physics* , 7597 (1996).
- ¹¹⁷T. Hollebeek, T.-S. Ho, and H. Rabitz, *Annual review of physical chemistry* **50**, 537 (1999).
- ¹¹⁸T. P. Senftle, S. Hong, M. M. Islam, S. B. Kylasa, Y. Zheng, Y. K. Shin, C. Junkermeier, R. Engel-Herbert, M. J. Janik, H. M. Aktulga, *et al.*, *npj Computational Materials* **2**, 1 (2016).
- ¹¹⁹P. Virtanen, R. Gommers, T. E. Oliphant, M. Haberland, T. Reddy, D. Cournapeau, E. Burovski, P. Peterson, W. Weckesser, J. Bright, *et al.*, *Nature methods* **17**, 261 (2020).
- ¹²⁰L. Ruddigkeit, R. V. Deursen, L. C. Blum, and J.-L. Reymond, *Journal of chemical information and modeling* **52**, 2864 (2012).
- ¹²¹G. H. Vineyard, *Journal of Physics and Chemistry of Solids* **3**, 121 (1957).
- ¹²²T. A. Halgren and W. N. Lipscomb, *Chemical Physics Letters* **49**, 225 (1977).
- ¹²³A. Goodrow, A. T. Bell, and M. Head-Gordon, *The Journal of chemical physics* **130**, 244108 (2009).
- ¹²⁴A. Denzel and J. Kastner, *Journal of chemical theory and computation* **14**, 5777 (2018).
- ¹²⁵Y. Yang, S. Zhang, K. D. Ranasinghe, O. Isayev, and A. E. Roitberg, *Annual Review of Physical Chemistry* **75**, 371 (2024).
- ¹²⁶D. Hao, X. He, A. E. Roitberg, S. Zhang, and J. Wang, *Journal of Chemical Theory and Computation* **18**, 978 (2022).
- ¹²⁷J. Behler, *Chemical Reviews* **121**, 10037 (2021).
- ¹²⁸E. Kocer, T. W. Ko, and J. Behler, *Annual review of physical chemistry* **73**, 163 (2022).
- ¹²⁹S. Manzhos and T. Carrington Jr, *Chemical Reviews* **121**, 10187 (2020).
- ¹³⁰J. Behler, *Angewandte Chemie International Edition* **56**, 12828 (2017).
- ¹³¹A. H. Larsen, J. J. Mortensen, J. Blomqvist, I. E. Castelli, R. Christensen, M. Duřak, J. Friis, M. N. Groves, B. Hammer, C. Hargus, *et al.*, *Journal of Physics: Condensed Matter* **29**, 273002 (2017).
- ¹³²H. B. Schlegel, *Journal of Computational Chemistry* **24**, 1514 (2003).
- ¹³³P. Virtanen, R. Gommers, T. E. Oliphant, M. Haberland, T. Reddy, D. Cournapeau, E. Burovski, P. Peterson, W. Weckesser, J. Bright, *et al.*, *Nature Methods* **17**, 261 (2020).
- ¹³⁴J. Baker and F. Chan, *Journal of Computational Chemistry* **17**, 888 (1996).
- ¹³⁵A. B. Birkholz and H. B. Schlegel, *Journal of Computational Chemistry* **36**, 1157 (2015).
- ¹³⁶S. Smidstrup, A. Pedersen, K. Stokbro, and H. Jónsson, *The Journal of Chemical Physics* **140** (2014).
- ¹³⁷P. Virtanen, R. Gommers, T. E. Oliphant, M. Haberland, T. Reddy, D. Cournapeau, E. Burovski, P. Peterson, W. Weckesser, J. Bright, S. J. van der Walt, M. Brett, J. Wilson, K. J. Millman, N. Mayorov, A. R. J. Nelson, E. Jones, R. Kern, E. Larson, C. J. Carey, Í. Polat, Y. Feng, E. W. Moore, J. VanderPlas, D. Laxalde, J. Perktold, R. Cimrman, I. Henriksen, E. A. Quintero, C. R. Harris, A. M. Archibald, A. H. Ribeiro, F. Pedregosa, P. van Mulbregt, and SciPy 1.0 Contributors, *Nature Methods* **17**, 261 (2020).
- ¹³⁸J. Simons, P. Joergensen, H. Taylor, and J. Ozment, *The Journal of Physical Chemistry* **87**, 2745 (1983).
- ¹³⁹S. Choi, *Nature Communications* **14**, 1168 (2023).